Causality, response theory, and the second law of thermodynamics

Denis J. Evans and Debra J. Searles
Research School of Chemistry, Australian National University, Canberra, Australian Capital Territory 0200, Australia
(Received 24 October 1995)

We show that there is a close connection between the assumption of causality and the second law of thermodynamics. We also show that for a class of classical reversible deterministic systems it is overwhelmingly improbable either to find causal steady states that violate the second law, or anticausal states that satisfy the second law. These arguments indicate that the existence of (and the sign associated with) the second law of thermodynamics is ultimately determined by causality. Our discussion employs a Green-Kubo relation that we derive for an anticausal linear transport coefficient. [S1063-651X(96)11205-8]

PACS number(s): 05.20.−y, 47.10.+g

I. INTRODUCTION

We live in a universe where cause precedes effect. This is in spite of the fact that the equations of motion, whether classical or quantum mechanical, are time reversible, and it is therefore dynamically possible for effect to precede cause. In our attempts to model the macroscopic behavior of the world around us, we describe apparently irreversible behavior such as heat or momentum flows by using causal constitutive relations.

In the 1950s and 1960s fluctuation relations—the so-called Green-Kubo relations—were derived for the causal transport coefficients that are defined by causal linear constitutive relations such as Fourier's law of heat flow or Newton's law of viscosity [1–4]. The Mori-Zwanzig projection operator formalism shows that the Green-Kubo relations for causal linear transport coefficients are a direct consequence of the equations of motion. Some years ago an objection to the derivation of Green-Kubo relations by linear response theory was raised by van Kampen [5]. However, this objection has more recently been dismissed by Morriss *et al.* [6].

It would thus seem that the derivation of Green-Kubo relations, which give a unique sign for each of the Navier-Stokes transport coefficients, constitutes a proof of the irreversibility of macroscopic behavior. The argument would run as follows: the Green-Kubo relations are derived using a self-consistent procedure; they lead directly to equilibrium fluctuation relations for the transport coefficients; these expressions have a unique sign; therefore the derivation of Green-Kubo relations shows that the universe is macroscopically asymmetric with respect to time reversal. Although Green-Kubo relations do not indicate the sign of the transport coefficient, they do indicate that the transport coefficient has a definite sign.

Recently we provided a simple argument that if a deterministically and reversibly thermostatted system which is initially at equilibrium is subject to a perturbing external field, then it becomes overwhelmingly probable to observe initial equilibrium microstates that subsequently generate nonequilibrium steady states that satisfy the second law [7]. This argument is based on the Boltzmann ansatz (that in the equilibrium microcanonical ensemble the probability of observing microstates within a specified phase space volume is proportional to the magnitude of that volume), and on the assumption of causality.

In this paper we show that if we derive Green-Kubo relations for the corresponding transport coefficients defined by *anticausal* constitutive relations the following hold: first, these antitransport coefficients have a sign opposite to their causal counterparts, and, second, it becomes overwhelmingly likely to observe anticausal nonequilibrium steady states that violate the second law. This argument, again based on the Boltzmann ansatz, shows that in an anticausal world it becomes overwhelmingly probable to observe *final* equilibrium microstates that evolved from nonequilibrium steady states that violate the second law. Although this behavior is not seen in the macroscopic world, *anticausal* behavior is permitted by the solution of the time reversible laws of dynamics, and we demonstrate, using computer simulation, how to find phase space trajectories which exhibit *anticausal* behavior.

II. CAUSAL AND ANTICAUSAL CONSTITUTIVE RELATIONS

Consider the component of the linear response at time t_1, $\delta B(t_1)$, of a system characterized by a response function $L(t_1,t_2)$. The response is due to the application of an external force F, acting for an infinitesimal time $\delta t_2(>0)$, at time t_2,

$$\delta B(t_1)=L(t_1,t_2)F(t_2)\delta t_2. \tag{1}$$

This is the most general scalar linear relation between the response and the force components. If the response of the system is independent of the time at which the experiment is performed [i.e., if the same response is generated when both times appearing in (1) are translated by an amount $\tau: t_2\rightarrow t_2+\tau$, $t_1\rightarrow t_1+\tau$], it is trivial to show that the response function $L(t_1,t_2)$ is solely a function of the difference between the times at which the force is applied and the response is monitored,

$$\delta B(t_1)=L(t_1-t_2)F(t_2)\delta t_2. \tag{2}$$

The invariance of the response to time translation is called the assumption of stationarity. Equation (2) does not in fact describe the results of actual experiments because it allows the response at time t_1 to be influenced not only by forces in the past, $F(t_2)$, where $t_2<t_1$, but also by forces that have not

yet been applied, $t_2 > t_1$ [8]. We therefore distinguish between the causal and anticausal response components,

$$\delta B_C(t_1) \equiv +L_C(t_1-t_2)F(t_2)\delta t_2, \quad t_1 > t_2,$$
$$\delta B_A(t_1) \equiv -L_A(t_1-t_2)F(t_2)\delta t_2, \quad t_1 < t_2. \tag{3}$$

Of course in actual laboratory experiments the anticausal response cannot easily be seen. Below, we will prove that $L_C(t) = L_A(-t)$.

Considering the response at time t to be a linear superposition of influences due to the external field at all possible previous (or future) times gives

$$B_C(t) = \int_{-\infty}^{t} L_C(t-t_1)F(t_1)dt_1 \tag{4}$$

for the causal response, and

$$B_A(t) = -\int_{t}^{+\infty} L_A(t-t_1)F(t_1)dt_1 \tag{5}$$

for the anticausal response.

III. GREEN-KUBO RELATIONS FOR THE CAUSAL AND ANTICAUSAL LINEAR RESPONSE FUNCTIONS

To make this discussion more concrete we will discuss Green-Kubo relations for shear viscosity [1]. Analogous results can be derived for each of the Navier-Stokes transport coefficients. We assume that the regression of fluctuations in a system at equilibrium, whose constituent particles obey Newton's equations of motion, are governed by the Navier-Stokes equations. We consider the wave vector dependent transverse momentum density

$$J_\perp(k_y,t) \equiv \sum_i p_{xi}(t) e^{ik_y y_i(t)}, \tag{6}$$

where p_{xi} is the x component of the momentum of particle i, y_i is the y coordinate of particle i, and k_y is the y component of the wave vector. The (Newtonian) equations of motion can be used to calculate the rate of change of the transverse momentum density. They give

$$\dot{J}_\perp = ik_y \left[\sum_i p_{xi} p_{yi} e^{ik_y y_i} + \tfrac{1}{2} \sum_{i,j} y_{ij} F_{xij} \frac{1-e^{ik_y y_{ij}}}{ik_y y_{ij}} e^{ik_y y_i} \right]$$
$$\equiv ik_y P_{yx}(k_y,t). \tag{7}$$

In this equation F_{xij} is the x component of the force exerted on particle i by particle j, $y_{ij} \equiv y_j - y_i$, and P_{yx} is the yx component of the pressure tensor.

We now consider the response of the pressure tensor to a strain rate γ, applied to the fluid for $t > 0$ in the causal system and for $t < 0$ in the anticausal system. Since the pressure tensor is related to the time derivative of the transverse momentum current by (7), and the strain rate is related to the Fourier transform of the transverse momentum density by $\gamma(k_y,t) = -ik_y J_\perp(k_y,t)/\rho$, the most general linear, stationary, and causal constitutive relation can be written as

$$\dot{J}_\perp(k_y,t) = \frac{-k_y^2}{\rho} \int_0^t \eta_C(k_y, t-s) J_\perp(k_y,s) ds, \quad t > 0, \tag{8}$$

where η_C is the causal response function (or memory function) and ρ is the density. The corresponding anticausal relation is

$$\dot{J}_\perp(k_y,t) = \frac{k_y^2}{\rho} \int_t^0 \eta_A(k_y, t-s) J_\perp(k_y,s) ds, \quad t < 0, \tag{9}$$

where η_A is the anticausal response function. Note that because $t < 0$, we find that the argument $(t-s)$ in (9) is less than zero, and we are indeed exploring the response of the system to a strain rate that is yet to be imposed.

It is straightforward to use standard techniques to evaluate the Green-Kubo relations for the causal and anticausal shear viscosity coefficients. In the anticausal case it is important to remember that the usual Laplace transform

$$\tilde{F}(s) \equiv \int_0^{+\infty} F(t) e^{-st} dt, \quad t \geq 0 \tag{10}$$

is inappropriate, and needs to be replaced by an anti-Laplace transform

$$\hat{F}(s) \equiv \int_{-\infty}^{0} F(t) e^{st} dt, \quad t \leq 0. \tag{11}$$

[Note: $\hat{F}(s) = \int_0^\infty F(-t) e^{-st} dt = \tilde{F}'(s)$, $t \geq 0$, where $F'(t) \equiv F(-t)$.] Using the fact that the anti-Laplace transform of a time derivative is $\hat{\dot{F}}(s) = F(0) - s\hat{F}(s)$, and that the anti-Laplace transform of a convolution is the product of the anti-Laplace transforms of the convolutes, one can easily derive the following relations for the shear viscosity and the anticausal shear viscosity:

$$\tilde{C}(k_y,s) = \frac{C(k_y,0)}{s + \dfrac{k_y^2 \tilde{\eta}_C(k_y,s)}{\rho}}, \quad \hat{C}(k_y,s) = \frac{C(k_y,0)}{s + \dfrac{k_y^2 \tilde{\eta}_A(k_y,s)}{\rho}}, \tag{12}$$

where

$$C(k_y,t) \equiv \langle J_\perp(k_y,t) J_\perp(-k_y,0) \rangle, \quad \forall t. \tag{13}$$

More useful relations for the viscosity coefficients, especially at $k = 0$, can be obtained by utilizing the equilibrium stress autocorrelation function

$$N(k_y,t) \equiv \frac{1}{Vk_BT} \langle P_{yx}(k_y,t) P_{yx}(-k_y,0) \rangle, \quad \forall t. \tag{14}$$

Using the fact that $\hat{N} = -\hat{\dot{C}}/k_y^2 V k_B T$, one can show [1,9]

$$\tilde{\eta}_C(k_y,s)=\frac{\tilde{N}(k_y,s)}{1-k_y^2\tilde{N}(k_y,s)/\rho s},$$

$$\tilde{\eta}_A(k_y,s)=\frac{\hat{N}(k_y,s)}{1-k_y^2\hat{N}(k_y,s)/\rho s}. \tag{15}$$

At zero wave vector, we find that the causal and anticausal memory functions are both given by the equilibrium autocorrelation function of the pressure tensor,

$$\eta_C(t)=\eta_A(-t) \quad \text{where } t>0$$
$$\equiv \eta(t)=\frac{V}{k_BT}\langle P_{yx}(t)P_{yx}(0)\rangle, \quad \forall t \tag{16}$$

where we have used $P_{yx}(t)V=\lim_{k\to 0}P_{yx}(k_y,t)$. Since equilibrium autocorrelation functions are symmetric in time, one does not have to distinguish between the positive and negative time domains. This proves, at least for shear viscosity, our contention made in Sec. II that $L_C(t)=L_A(-t)$.

Using Eqs. (7)–(9) and taking the zero wave vector limit, we obtain the causal response of the yx component of the pressure tensor,

$$P_{yxC}(t)=-\int_0^t \eta(t-s)\gamma(s)ds, \quad t>0, \tag{17}$$

and the anticausal response is

$$P_{yxA}(t)=\int_t^0 \eta(t-s)\gamma(s)ds, \quad t<0. \tag{18}$$

In the linear regime close to equilibrium the entropy production per unit time, dS/dt, is given by

$$\frac{dS}{dt}=-P_{yx}(t)\gamma(t)V, \tag{19}$$

where $\gamma(t)$ is the time dependent strain rate. From Eqs. (17) and (18), it is easy to see that if we conduct two shearing experiments, one on a causal system with a strain rate history $\gamma_C(t)$ and one on an anticausal system with $\gamma_A(t)=\pm\gamma_C(-t)$, then

$$\left.\frac{dS(t)}{dt}\right|_A=\left.\frac{-dS(-t)}{dt}\right|_C. \tag{20}$$

This proves that if the causal system satisfies the second law of thermodynamics, then the anticausal system must violate that law, and vice versa.

IV. EXAMPLE: THE MAXWELL MODEL OF VISCOSITY

In this section we examine the consequences of the causal and anticausal responses by considering the Maxwell model for linear viscoelastic behavior [1]. If we consider the causal response of a system to a two step strain rate ramp,

$$\gamma_C(t)=a, \quad 0<t<t_1,$$
$$\gamma_C(t)=b, \quad t_1<t<t_2, \tag{21}$$

then use the Maxwell memory kernel

$$\eta(t)=G_\infty e^{-|t|/\tau}, \quad \forall t \tag{22}$$

in (17) and the fact that the causal η_C and anticausal η_A Maxwell shear viscosities in the zero frequency limit are

$$\eta_C=\eta_A=G_\infty\tau=\eta, \tag{23}$$

we find that the causal response is

$$P_{xyC}(t)=-a\,\eta(1-e^{-t/\tau}), \quad 0<t<t_1,$$
$$P_{xyC}(t)=-a\,\eta(e^{-(t-t_1)/\tau}-e^{-t/\tau})-b\,\eta(1-e^{-(t-t_2)/\tau}), \tag{24}$$
$$t_1<t<t_2.$$

If we now consider the corresponding anticausal experiment with strain rate histories given by

$$\gamma_A(t)=a, \quad -t_1<t<0,$$
$$\gamma_A(t)=b, \quad -t_2<t<-t_1, \tag{25}$$

we find that the anticausal response is

$$P_{xyA}(t)=a\,\eta(1-e^{t/\tau}), \quad -t_1<t<0,$$
$$P_{xyA}(t)=a\,\eta(e^{(t+t_1)/\tau}-e^{t/\tau})+b\,\eta(1-e^{(t+t_2)/\tau}), \tag{26}$$
$$-t_1<t<-t_2.$$

From Eqs. (24) and (26), it is clear that

$$P_{xyA}(t)=-P_{xyC}(-t). \tag{27}$$

These response functions are shown graphically in Fig. 1. A two step strain rate ramp with $a=1.0$, $b=0.5$, $t_1=2$, and $t_2=4$ was considered. Equations (24) and (26) were used to predict the causal and anticausal responses, respectively, of the xy component of the pressure tensor. Values of $G_\infty=40.0$ and $\tau=0.05$ were used in the model. These values were obtained from approximate fits to computer simulation data (see Sec. V).

The data in Fig. 1 show that for the causal response, P_{xy} is zero at equilibrium ($t\leqslant 0$) and decreases when the field is applied until the steady state value is obtained. It remains at the steady value until $t=2$, at which time the strain rate is reduced. Since this system is causal, no change in P_{xy} occurs until *after* the strain rate is reduced, when it increases until the system reaches a different steady state. We display the anticausal response from $t=-4$, where it is in an antisteady state. Just *before* the strain rate is increased (at $t=-2$), P_{xy} increases to another antisteady state value. Using Eq. (19) we see that the causal response is entropy increasing and satisfies the second law, whereas the anticausal response is entropy decreasing and violates the second law.

V. PHASE SPACE TRAJECTORIES FOR SHEAR FLOW

We now examine the causal and anticausal responses on a microscopic scale, and consider the relative probability of observing causal and anticausal trajectories by studying a thermostatted system of N particles under shear. In this sys-

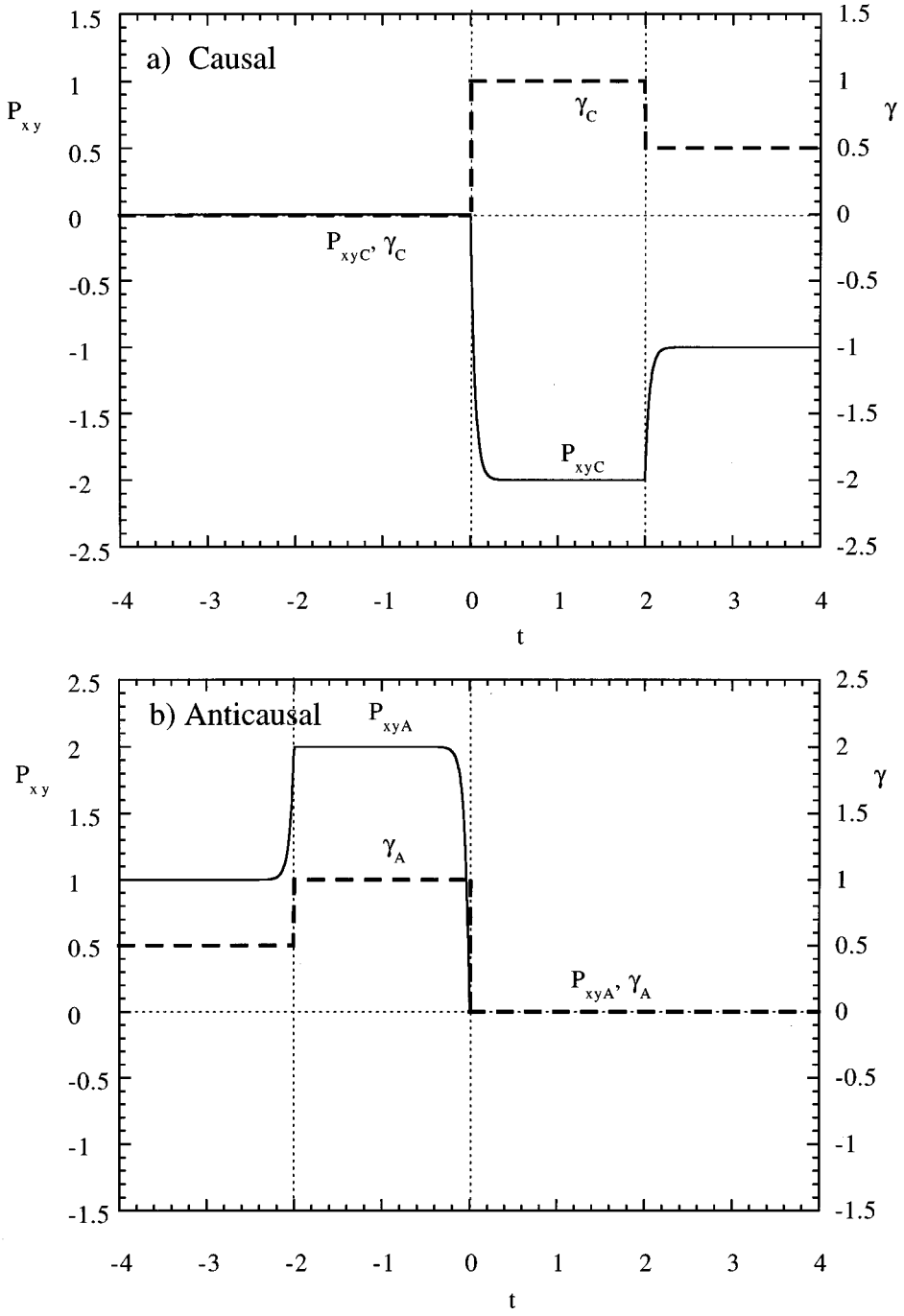

FIG. 1. The (a) causal and (b) anticausal response of P_{xy} to a two step strain rate ramp determined using the Maxwell model for linear viscoelastic behavior with $G_\infty=40$ and $\tau=0.05$ (solid line). In both cases the time dependence of the strain rate is shown as a dashed line.

tem the external field is the shear rate $\partial u_x/\partial y=\gamma(t)$ (the y gradient of the x-streaming velocity) and the shear stress $-P_{xy}$ times the system volume V is the dissipative flux $-J$ [1]. The equations of motion for the particles are given by the so-called [1] thermostatted Sllod equations

$$\dot{\mathbf{q}}_i=\mathbf{p}_i/m+\mathbf{i}\gamma y_i\,,\quad \dot{\mathbf{p}}_i=\mathbf{F}_i-\mathbf{i}\gamma p_{yi}-\alpha\mathbf{p}_i\,. \tag{28}$$

At arbitrary strain rates these equations give an exact description of adiabatic Couette flow. This is because the adiabatic Sllod equations for a step function strain rate $\partial u_x(t)/\partial y=\gamma(t)=\gamma\Theta(t)$, are equivalent [1] to Newton's equations after the imposition of a linear velocity gradient at $t=0$ [i.e., $d\mathbf{q}_i(0^+)/dt=d\mathbf{q}_i(0^-)/dt+\mathbf{i}\gamma y_i$]. At a low Reynolds number, the momenta $\mathbf{p}_i$ are peculiar momenta, and α is determined using Gauss's principle of least constraint to keep the internal energy $H_0=\Sigma p_i^2/2m+\Phi(q)$ fixed [1]. Thus

$$\alpha=-\gamma\left[\sum_{i=1}^{N} p_{xi}p_{yi}/m-\tfrac{1}{2}\sum_{i,j}^{N} x_{ij}F_{yij}\right]\Bigg/\sum_{i=1}^{N} p_i^2/m$$
$$=-P_{xy}\gamma V\Bigg/\sum_{i=1}^{N} p_i^2/m, \tag{29}$$

where F_{yij} is the y component of the intermolecular force exerted on particle i by j and $x_i\equiv x_j-x_i$.

The thermostatted Sllod equations of motion (28) and (29) are time reversible [1]. Therefore for every i segment $\Gamma_{(i)}(t)$,

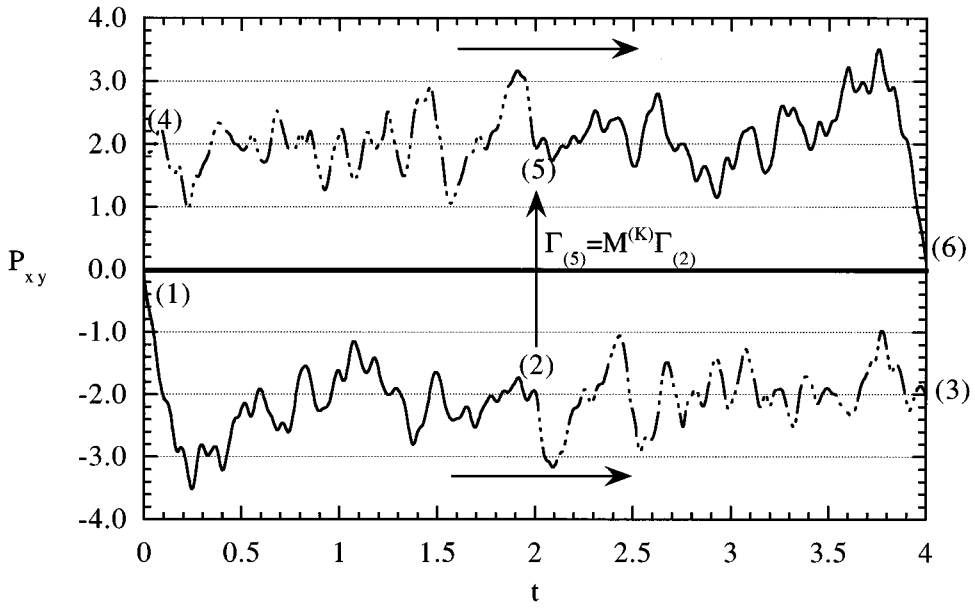

FIG. 2. P_{xy} for trajectory segments from a simulation of 200 disks at $T=1.0$ and $n=0.8$. A constant strain rate of $\gamma=1.0$ is applied at $t=0$. The trajectory segment $\mathbf{\Gamma}_{(1,3)}$ was obtained from a forward time simulation. At $t=2$, a K map was applied to $\mathbf{\Gamma}_{(2)}$ to give $\mathbf{\Gamma}_{(5)}$. Forward and reverse time simulations from this point give the trajectory segment $\mathbf{\Gamma}_{(5,6)}$ and $\mathbf{\Gamma}_{(5,4)}$, respectively. If one inverts P_{xy} in $P_{xy}=0$ and inverts time about $t=2$, one transforms the $P_{xy}(t)$ values for the antisegment $\mathbf{\Gamma}_{(4,6)}$ into those for the conjugate segment $\mathbf{\Gamma}_{(1,3)}$.

$(0<t<\tau)$, there exists a conjugate trajectory segment $\mathbf{\Gamma}_{(i^K)}(t)$, $(0<t<\tau)$ with the property that $P_{xy}(\mathbf{\Gamma}_{(i^K)}(t))=-P_{xy}(\mathbf{\Gamma}_{(i)}(-t))$, $(0<t<\tau)$. Thus the τ-averaged shear stress $\langle P_{xy}\rangle_{\tau,(i)}\equiv 1/\tau\int_0^\tau P_{xy}(\mathbf{\Gamma}_{(i)}(s))ds$ for segment i is equal and opposite to that for its conjugate: $\langle P_{xy}\rangle_{\tau,(i^K)}=-\langle P_{xy}\rangle_{\tau,(i)}$ [7]. We note that since the solution of the equations of motion is a unique function of the initial conditions, the conjugate segment is also unique.

We have previously shown that for shear flow conjugate segments may be generated by using a phase space mapping known as a Kawasaki or K map [1]. A K map of a phase $\mathbf{\Gamma}$ is defined as a time-reversal map which is followed by a y reflection. In the case of shear flow the K map leaves the strain rate unchanged but changes the sign of the shear stress, that is $M^K\mathbf{\Gamma}=M^K(x,y,z,p_x,p_y,p_z,\gamma)=(x,-y,z,-p_x,p_y,-p_z,\gamma)\equiv\mathbf{\Gamma}^{(K)}$ [1]. It is straightforward to show that the Liouville operator for the system (28) and (29), $iL(\mathbf{\Gamma},\gamma)\equiv\Sigma[\dot{\mathbf{q}}_i(\mathbf{\Gamma})\cdot\partial/\partial\mathbf{q}_i+\dot{\mathbf{p}}_i(\mathbf{\Gamma})\cdot\partial/\partial\mathbf{p}_i]$, has the property that under a K map $M^KiL(\mathbf{\Gamma},\gamma)=iL(\mathbf{\Gamma}^{(K)},\gamma^{(K)})=-iL(\mathbf{\Gamma},\gamma)$ [1]. If we assume a strain rate history such that $\gamma_K(-t)=\gamma(t)$ $\forall t$, then it follows that if a K map is carried out on an arbitrary phase $\mathbf{\Gamma}$ at $t=0$ then evolution *forward* in time from $\mathbf{\Gamma}^{(K)}$ under a strain rate $\gamma_K(t)$ is equivalent to time evolution *backwards* in time from $\mathbf{\Gamma}$ under the strain rate history $\gamma(t)$ $(t<0)$,

$$P_{xy}(-t,\mathbf{\Gamma},\gamma(-t))=\exp[-iL(\mathbf{\Gamma},\gamma(-t))t]P_{xy}(\mathbf{\Gamma})=-P_{xy}(t,\mathbf{\Gamma}^{(K)},\gamma_K(t)). \quad (30)$$

We note that if we do not assume that $\gamma_K(-t)=\gamma(t)$ $\forall t$, then there is no general method for generating conjugate trajectory segments. This is because propagators with different strain rates do not commute, and the inverse propagator must therefore retrace the strain rate history of the conjugate propagator in inverse historical order.

If the original segment $\mathbf{\Gamma}(t)$ was causal with systematic increases in shear stress $-P_{xy}$ occurring *after* increases in strain rate, then the forward mapped segment $\mathbf{\Gamma}^{(K)}(t)$ $(t>0)$ will necessarily be anticausal with systematic increases in shear stress occurring *before* the corresponding increases in strain rate, $\gamma_K(t)$ $(t>0)$.

We will now indicate in more detail how to construct the conjugate segment $i^{(K)}$ from an arbitrary phase space trajectory segment i [7]. The construction is illustrated in Fig. 2 for the case where the strain rate remains the same for the duration of the trajectory. A trajectory of length 2τ is generated by solving the equations of motion. The conjugate segment is then constructed by applying a K map to the phase at the midpoint of the segment $(t=\tau)$ $M^K\mathbf{\Gamma}_{(2)}=\mathbf{\Gamma}_5$. We then advance in time from the point $(\mathbf{\Gamma}_{(5)})$, to $t=2\tau$, by solving the equations of motion and also go backwards in time from the K-mapped point $t=\tau$, to $t=0$. A conjugate trajectory of length 2τ is thereby produced. This construction has previously been described in more detail [7].

Clearly, the mapped trajectory is a solution of the equations of motion for the system. When the K map is carried out at $t=0$, the shear stress is inverted, and Eq. (30) shows that $P_{xy}(t+\tau,\mathbf{\Gamma})=-P_{xy}(t-\tau,\mathbf{\Gamma}^{(K)})$ and similarly $P_{xy}(t-\tau,\mathbf{\Gamma})=-P_{xy}(t+\tau,\mathbf{\Gamma}^{(K)})$; therefore, for every point on the original trajectory there is a unique point on the mapped trajectory with opposite shear stress. The τ-averaged shear stress of the conjugate trajectory is opposite to that of the original trajectory, that is $\langle P_{xy}\rangle_{t,(i^K)}=-\langle P_{xy}\rangle_{\tau,(i)}$. Thus if the original segment satisfied the second law, then the conjugate segment violates the second law, and vice versa.

In a causal world, which is described by causal macroscopic constitutive relations such as (4), observed segments are overwhelmingly likely to satisfy the second law. We can show this by discussing the ratio of probabilities of finding the initial phases, $\mathbf{\Gamma}_{(1)}$ and $\mathbf{\Gamma}_{(4)}$ in Fig. 2, which generate these conjugate segments. In a causal world, the probabilities of observing the segments $\mathbf{\Gamma}_{(1,3)}$ and $\mathbf{\Gamma}_{(4,6)}$ are of course proportional to the probabilities of observing the *initial* phases which generate those segments. [Note that we denote the trajectory τ segment $\mathbf{\Gamma}_{(i)}\rightarrow\mathbf{\Gamma}_{(j)}=\mathbf{\Gamma}_i(\tau)$ by $\mathbf{\Gamma}_{(ij)}$.] It is convenient to consider a small phase space volume $V(\mathbf{\Gamma}_{(i)}(0))$ about an initial phase $\mathbf{\Gamma}_{(i)}(0)$. Because

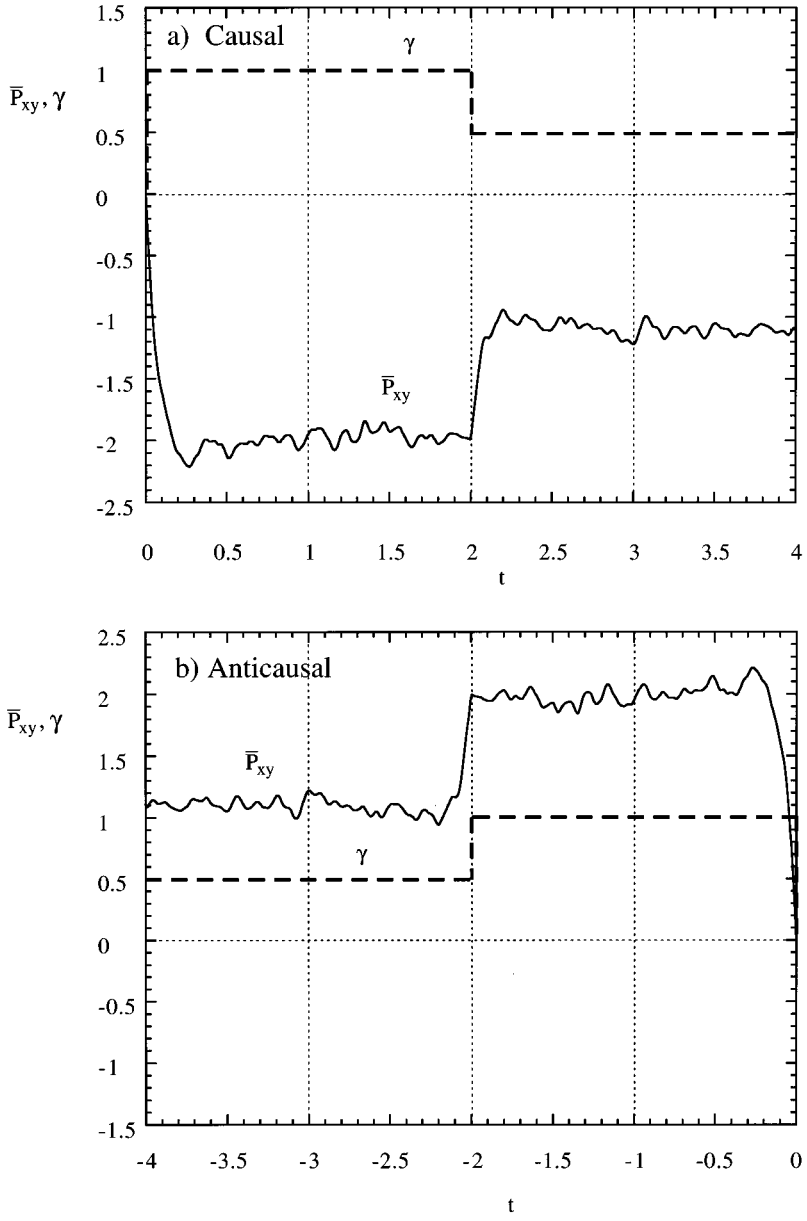

FIG. 3. $\overline{P_{xy}}$ (solid line) from nonequilibrium molecular dynamics simulations of 56 particles at $T=1.0$ and $n=0.8$ undergoing shear flow. The dashed line gives the time dependence of the strain rate. In (a), P_{xy} was determined using 100 trajectories whose initial phases were selected from an equilibrium distribution, and to which a two step strain rate was applied. (b) shows P_{xy} for their conjugate trajectories. The conjugate trajectories were obtained by applying a K map to the phase of the trajectory at $t=2$, simulating forward and backward in time from this point and translating in time so that the conjugate trajectory ends at $t=0$. Note that the strain rate history of the conjugate trajectory is reversed.

the initial phases are distributed *microcanonically*, the probability of observing ensemble members inside $V(\mathbf{\Gamma}_{(i)}(0))$, is proportional to $V(\mathbf{\Gamma}_{(i)}(0))$. From the Liouville equation $df(\mathbf{\Gamma},t)/dt=3N\alpha(\mathbf{\Gamma})f(\mathbf{\Gamma},t)+O(1)$ and the fact that, for sufficiently small volumes, $V(\mathbf{\Gamma}(t))\sim 1/f(\mathbf{\Gamma}(t),t)$, we can make the following observations:

$$V_2=V_1(\tau)=V_1(0)\ \exp\left[-\int_0^{\tau}3N\alpha(s;\mathbf{\Gamma}_1)ds\right]$$

and

$$V_3=V_1(2\tau)=V_1(0)\ \exp\left[-\int_0^{2\tau}3N\alpha(s;\mathbf{\Gamma}_{(1)})ds\right],$$

where $\alpha(s;\mathbf{\Gamma}_{(1)})$ denotes $\alpha(s)$ computed along a segment that begins, at $s=0$, at $\mathbf{\Gamma}_{(1)}(0)$.

Since the segment $\mathbf{\Gamma}_{(4,6)}$ is related to $\mathbf{\Gamma}_{(1,3)}$ by a K map which is applied at $t=\tau$, and the Jacobian of the K mapping is unity, $V_2=V_5$, $V_3=V_4$, and $V_1(0)=V_6$. However, since $V_1(0)$ and V_4 are volumes at $t=0$ and the distribution of initial phases is microcanonical, we can compute the ratio of probabilities μ_{i*}, μ_i of observing, in a causal world, $t=0$ phases within $V_4(0)$ and V_1. This ratio is just the volume ratio

$$\mu_{i*}/\mu_1=V_4/V_1(0)=V_1(2\tau)/V_1(0)$$
$$=\exp\left[\int_0^{2\pi}-3N\alpha(s;\mathbf{\Gamma}_{(1)})ds\right],\quad \forall\tau. \qquad (31)$$

Thus if the world is causal and we assume segment $1(\equiv\mathbf{\Gamma}_{(1,3)})$ satisfies the second law, then $\langle\alpha\rangle_{\tau,(1,3)}>0$ and $\mu_{1*}\mu_1\to 0$ (i.e., we overwhelmingly observe segment 1 rather than the antisegment 1^* which violates the second law). Conversely, if segment 1 violates the second law, then $\langle\alpha\rangle_{\tau,(1,3)}<0$ and $\mu_{1*}\mu_1\to\infty$ (i.e., we overwhelmingly see segment 1^* rather than antisegment 1 which violates the second law). Equation (31) has recently been verified by numerical simulations of a system undergoing shear flow [7].

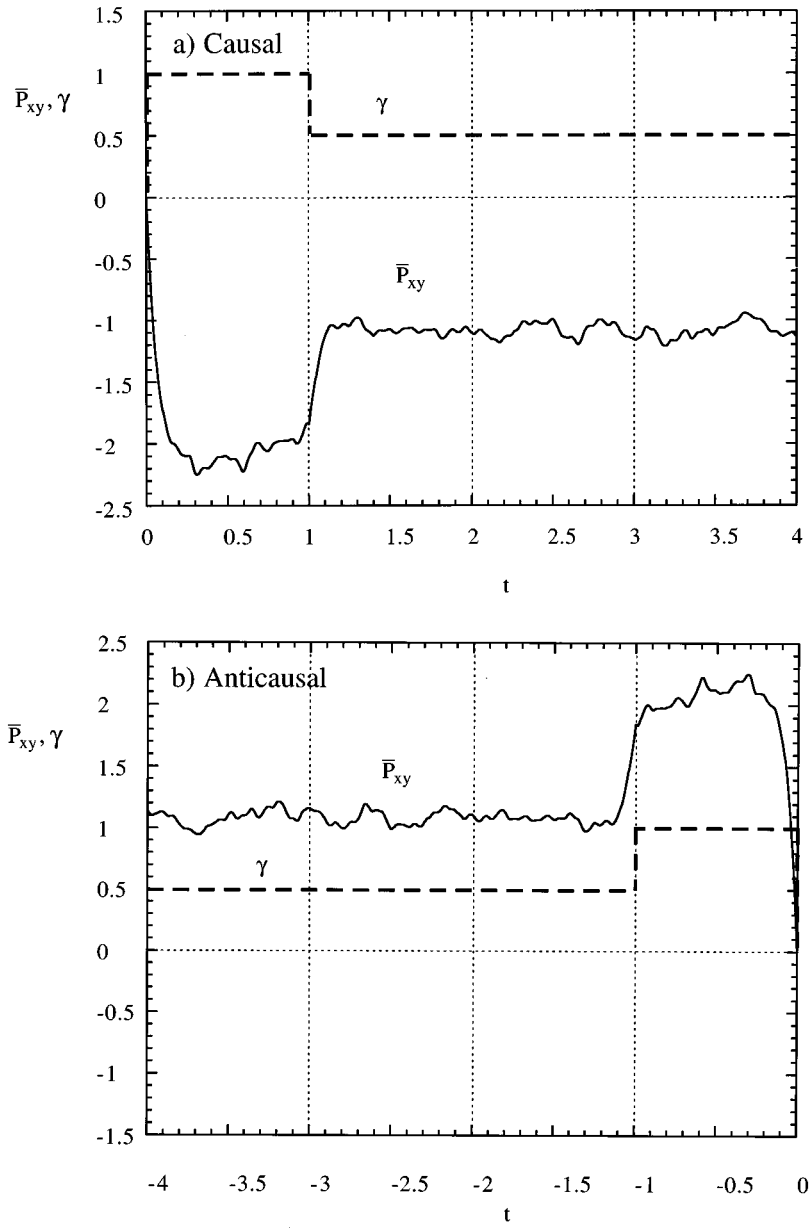

FIG. 4. The same as Fig. 3, but with a different two step strain rate ramp. (a) shows P_{xy} for trajectories sampled from an equilibrium distribution at $t=0$, and (b) shows P_{xy} for conjugate trajectories generated from the trajectories in (a). In both cases the time dependence of the strain rate is shown by a dashed line.

In an anticausal world where effects precede their causes, the probabilities of observing the segments $\mathbf{\Gamma}_{(1,3)}$ and $\mathbf{\Gamma}_{(4,6)}$ are proportional to the probabilities of observing the *final* phases generated by those segments. The system will be at equilibrium at the end point (rather than the beginning) of the trajectory segments and antisegments. It is trivial to see that in an anticausal world it would be overwhelmingly more probable to observe segments that violate the second law than segments that satisfy the second law. We do not make that argument here because it is a rather obvious extension of the argument given above for causal systems. Put simply, in order for a group of trajectory segments to have a large final equilibrium volume they have to violate the second law with an expanding (rather than shrinking) volume element.

VI. SIMULATION RESULTS

We can demonstrate the relationships between the conjugate pair trajectories, the second law of thermodynamics, and causal and anticausal responses using numerical simulations of the system described by Eqs. (28) and (29). Figure 2 shows the response of P_{xy} for a trajectory and its conjugate when a constant strain rate is applied. The response was determined using nonequilibrium molecular dynamics simulations of 200 disks in two Cartesian dimensions. The disks interact via the short range potential of Weeks, Chandler, and Andersen [10],

$$\phi(r)=\begin{cases}4(r^{-12}-r^{-6})+1, & r<2^{1/6}\\ 0, & r>2^{1/6}.\end{cases} \tag{32}$$

Shearing periodic boundary conditions were used to minimize boundary effects [1]. The system was maintained at a constant kinetic temperature of $T=1.0$ and the particle density was $n=N/V=0.8$. An initial phase was selected from an equilibrium distribution, and a strain rate of $\gamma=1.0$ was applied to the system at $t=0$. A trajectory segment was generated by simulating forward in time to $t=4$. The conjugate trajectory was constructed using the scheme described above. Examination of the trajectories shows that $P_{xy}(\tau+\mathrm{t})$ for the

trajectory satisfying the second law is equal in magnitude but opposite in sign to $P_{xy}(\tau - t)$ for the trajectory violating the second law, where τ is the time at which the K map is applied ($\tau = 2$). These results therefore verify the relationship between P_{xy} of trajectories satisfying the second law and conjugate trajectories violating the second law given by Eq. (30).

The causality of the response is more clearly demonstrated in Figs. 3 and 4, where the response of P_{xy} to different strain rate ramps is shown. $P_{xy}(t)$ was averaged over 100 individual trajectories to reduce the fluctuations in the steady state, and gave P_{xy}, a partially averaged response. In these simulations 56 disks were used. The initial phases of the trajectories shown in Figs. 3(a) and 4(a) were sampled from the equilibrium distribution at $t = 0$. Figure 3(a) shows the response of the shear stress of these trajectories to a strain rate of $\gamma = 1.0$ applied at $t = 0$, and reduced to $\gamma = 0.5$ at the midpoint of the trajectory ($t = 2$). To ensure that the high symmetry of the strain rate ramp does not influence the results, an alternative step strain rate ramp was considered. The response when the strain rate is reduced from $\gamma = 1.0$ to $\gamma = 0.5$ at $t = 1$ was simulated, and is shown in Fig. 4(a). In both cases, P_{xy} is zero at equilibrium and decreases to a steady state value after the field is applied. After the strain rate is reduced, P_{xy} increases to a different steady state value.

The conjugate trajectories are shown in Figs. 3(b) and 4(b). They were constructed as described above and translated in time to begin at $t = -4$. At this time, the system is in an antisteady state, and P_{xy} maintains its antisteady state value until just *before* the the strain rate is changed, when it increases to a different antisteady state value.

These response curves demonstrate that trajectories satisfying the second law only respond to the change in the strain rate *after* it is imposed and therefore they are *causal*. Conversely, the conjugate trajectories violating the second law respond to the step in the strain rate *before* it is made, so they are *anticausal*. Close inspection of the graphs reveals that at all points along individual pairs of conjugate trajectories, $P_{xy}(t)_{\text{trajectory}} = -P_{xy}(-t)_{\text{conjugate trajectory}}$, which follows from Eq. (30).

The system used in the simulations corresponds to that examined using the Maxwell model in Sec. IV. Figure 3 shows the response, determined by nonequilibrium molecular dynamics simulation, to the same two step strain rate ramp which was used to model the response shown in Fig. 1. Comparison of these response curves indicates that the system is reasonably well represented by the Maxwell model.

VII. CONCLUSION

We have derived a Green-Kubo relation for an anticausal linear transport coefficient. By comparing this relation with the corresponding relation for the conjugate causal transport coefficient we observe that if the causal transport coefficient satisfies the second law of thermodynamics, then the anticausal transport coefficient necessarily violates the second law. Further, we give an argument that in reversible, deterministic systems it is overwhelmingly improbable either to find causal steady states that violate the second law or to find anticausal states that satisfy the second law. This argument is based on the Boltzmann ansatz that at equilibrium in the microcanonical ensemble the probability of observing microstates within a given volume is proportional to the magnitude of that volume.

We have thus shown that there is a deep connection between causality and the second law of thermodynamics. We cannot violate the second law for long and still satisfy causality.

Finally we would like to remark that for dilute gases an analogous state of affairs exists with regard to the calculation of transport coefficients from the Boltzmann equation. The Boltzmann equation is time irreversible and leads to transport coefficients that satisfy the second law. This is analogous to Green-Kubo relations that satisfy the second law for linear transport coefficients in fluids of arbitrary density—Sec. III. In 1960 Cohen and Berlin [11] showed that if the *molecular chaos* assumption of Boltzmann is assumed to apply to *post-collisional* distributions rather than (as Boltzmann assumed) to *pre-collisional* distributions, one can derive an *anti-Boltzmann* equation (our terminology). This use of Boltzmann's molecular chaos assumption for precollisional and post-collisional distributions is analogous to our use of Boltzmann's ansatz before and after the strain rate ramps—Sec. V. The anti-Boltzmann equation derived by Cohen and Berlin obeys an anti-H theorem [11] which violates the second law. Consequently the anti-Boltzmann equation also leads to negative values for the Navier-Stokes transport coefficients.

ACKNOWLEDGMENTS

D.J.E. would like to thank the National Institute of Standards and Technology for partial support of this work. D.J.S. would like to thank the Australian Research Council for the award of an ARC Fellowship. D.J.E. would also like to thank Professor E. G. D. Cohen for initially raising the question of determining the sign of the Green-Kubo relations. The authors would like to thank Dr. G. P. Morriss for reading an early draft of this paper.

[1] D. J. Evans and G. P. Morriss, *Statistical Mechanics of Nonequilibrium Liquids* (Academic, London, 1990).
[2] M. S. Green, J. Chem. Phys. **22**, 398 (1954).
[3] R. Kubo, J. Phys. Soc. Jpn. **12**, 570 (1957).
[4] R. Zwanzig, Ann. Rev. Phys. Chem. **16**, 67 (1965).
[5] N. G. van Kampen, Phys. Norv. **5**, 279 (1971).
[6] G. P. Morriss, D. J. Evans, E. G. D. Cohen, and H. van Beijeren, Phys. Rev. Lett. **62**, 1579 (1989).
[7] D. J. Evans and D. J. Searles, Phys. Rev. B **50**, 1645 (1994).
[8] A. B. Pippard, *Response and Stability: An Introduction to the Physical Theory* (Cambridge University Press, Cambridge, 1985).
[9] J. P. Boon and S. Yip, *Molecular Hydrodynamics* (McGraw-Hill, New York, 1980).
[10] J. D. Weeks, D. Chandler, and H. C. Andersen, J. Chem. Phys. **54**, 5237 (1971).
[11] E. G. D. Cohen and T. H. Berlin, Physica **26**, 717 (1960).